Roll control of an autonomous underwater vehicle using an internal rolling mass

Eng You Hong and Mandar Chitre

Abstract A stable autonomous underwater vehicle (AUV) is essential for underwater survey activities. Previous studies have associated poor results in bathymetry survey and side-scan imaging with the vehicle's unwanted roll motion. The problem is becoming more prominent as AUVs are smaller nowadays. This causes reduction in the metacentric height of the AUVs which affects the inherent self-stabilization in the roll-axis. In this paper, we demonstrate the use of an internal rolling mass (IRM) mechanism to actively stabilize the roll motion of an AUV. We rotate the whole electronics tray, which has an off-centric center of gravity, to produce the required torque to stabilize the roll motion. The mechanical design of such mechanism and its dynamics modeling are discussed in detail. A Proportional-Integral (PI) controller is synthesized using the identified linear model. Results from tank tests and open-field tests demonstrate the effectiveness of the mechanism in regulating the roll motion of the AUV.

1 Introduction

A stable autonomous underwater vehicle (AUV) is essential for underwater surveys such as seafloor imaging using side-scan sonar, bathymetric mapping using multi-beam sonar, and photo mosaicking using underwater camera. As compared with yaw and pitch, the roll of a torpedo-shape AUV has a smaller moment of inertia and drag. So, the roll dynamics is oscillatory when the AUV is subjected to induced

Eng You Hong
ARL, Tropical Marine Science Institute, National University of Singapore, Singapore,
e-mail: tmseyh@nus.edu.sg

Mandar Chitre
Department of Electrical & Computer Engineering and ARL, Tropical Marine Science Institute, National University of Singapore, Singapore e-mail: mandar@nus.edu.sg

propeller torque, unknown disturbances and banking motion during turns. Without roll stabilization, the unwanted roll motion of an AUV can be problematic [7].

Singh, *et al.* [9], stated in their bathymetry paper, the roll bias is the most dominant error source as it directly affects the slope of the area being surveyed. Kirkwood, *et al.* [3] stated that the roll stability is critical to multibeam mapping and it is of high priority. For a side-scan sonar application, the AUV roll motion may cause layover to occur [10]; the affected samples are hard to interpret and need to be discarded. The unwanted roll motion can also affect both diving and steering performance of the AUV. This is due to the fact that most feedback controllers are designed on the assumption that yaw and pitch motion are decoupled. When the roll of the AUV is non-zero, the assumption is violated and thus the performance of a decoupled controller may be affected [6].

The problem is becoming more prominent as AUVs are smaller nowadays. Smaller AUVs are built in order to reduce manufacturing costs and ease deployment by one or two operators. Smaller AUVs pose constraints in placement of internal components and cause reduction in the metacentric height of the AUVs. This affects the inherent self-stabilization in the roll-axis. As a result, smaller AUVs are vulnerable to oscillatory roll motion.

In this study, we investigate the use of an internal rolling mass mechanism to actively stabilize the roll motion of an AUV. Internal actuators have few appealing features. Firstly, they can be used at low speeds where fins lose their usefulness. Secondly, they can be housed completely inside the vehicle and therefore are less prone to damage due to impact or corrosion [11]. Thirdly, they do not create external drag.

The use of an internal moving mass is not new in underwater vehicle applications. It has been used in underwater gliders such as SLOCUM, the Spray glider and the Seaglider [5]. The use of internal moving mass is also found in some AUVs. One example is the hybrid AUV – eFolaga [1] where the battery is moved along the longitudinal axis to provide pitch control. However, the use of an internal mass for roll control is rare because of the limited lateral space available for any significant linear motion. Furthermore, the use of linear motion requires a runway for the moving mass which is practically infeasible as the internal space already crowded with the essential components. We got around this limitation by designing a rolling mass mechanism that made use of the whole electronics tray (including batteries) as a moving mass.

The moving mass is capable of rotating with respect to the longitudinal axis of the AUV – hence we call it as an internal rolling mass (IRM) mechanism. The center of gravity (CG) of the IRM is off-centric. By rotating the IRM, we effectively change the CG of the AUV. By using the gravity force that acting through the CG, we can therefore generate the required torque to stabilize the roll dynamics.

In this paper, we tackle the unwanted roll motion through active roll stabilization by using the IRM mechanism. To the best of our knowledge, we are the first to report on the use of internal moving mass to stabilize the roll of an underactuated, tail-thrusted and fins-controlled AUV. We illustrate the design of the IRM mechanism by implementation on the STARFISH AUV [4]. The STARFISH AUV is a streamlined

AUV with a single thruster and four control surfaces at the tail. This is the most widely used configuration for AUVs in both commercial and research communities. Hence our discussion of the IRM mechanism is relevant and widely applicable to many AUVs in-use today.

This paper is organized as follows: In section 2, we illustrate the mechanical design of the IRM mechanism. This is followed by the modeling of the roll dynamics of the AUV which the IRM acts as an actuator in section 3. We present the results of system identification where parameters of the model were identified in section 4. In section 5, we show how controller was designed to regulate the roll motion. Experimental results are presented in section 6. Lastly, in section 7 we present the conclusions.

2 Mechanical Design

2.1 STARFISH AUV

The STARFISH AUVs are torpedo-shaped with 200 mm diameter. They are designed to be modular. The baseline STARFISH AUV consists of 3 basic sections - a nose section, a command & control section and a tail section. The total length is about 1.6 m and it weighs about 45 kg. Additional payload sections can be added to the baseline STARFISH AUV depending on the application. We currently have a Doppler Velocity Log (DVL) section, a side-scan sonar section and a chemical sensor section in our collection of payloads. The interested reader may refer to [4] for detailed discussions on the mechanical, electrical and software interfaces between the sections of the STARFISH AUV.

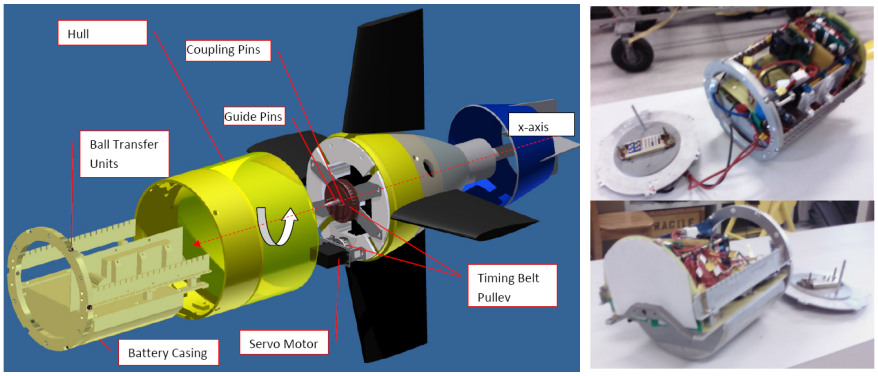

Fig. 1: Mechanical design of the Internal Rolling Mass (IRM) mechanism. Pictures on the right show the tail electronic tray which has a battery tray that attached to its bottom half.

2.2 Design Requirements

We need a mechanism that able to shift the CG of the AUV in the sway axis such that the roll equilibrium of the AUV can be changed by $\pm 5^{\circ}$. In order to shift the CG, we need some form of moving mass. So, it can be either a linear moving mass or a rotating mass. Our implementation using a rotating mass is illustrated in Fig. 1.

The actuation is provided by a servomotor mounted at the bottom end of the tail section through a bracket. It has a maximum torque of 1.92 Nm and maximum speed of 6.16 rad/s. Two timing belt pulleys are used for power transmission from the servomotor to the central axis. The drive pulley ratio is 1:2, thus increasing the output torque by a factor of two. Guide pins are used to guide the assembly of the whole tail tray (nickel bright in the figure) into the hull. Two coupling pins are used to transmit the torque from the central pulley to the tail tray. As the main mass of the tail tray is contributed by the battery placed in the bottom half, we effectively change the CG as the tail tray rolls inside the hull.

This design fulfills the following requirements :

2.2.1 Space Constraint

Constrained by the AUV diameter of 200 mm, there is no sufficient runway for a linear moving mass to have an effective change in CG. In addition, the existing components, such as electronics and battery, have already taken up most of the space in the tail section. So, without affecting components in other AUV's sections, we consolidate all the existing components in the tail section onto a tail tray, and make the tail tray as our moving mass. We were able to find space for a servomotor, two pulleys and a timing belt without making changes to the existing tail section hull (such as elongate it).

2.2.2 Energy Consumption

By having the mechanism at the tail section, we make use of the existing micro-controller to control the servomotor. The same micro-controller is used for thruster and fins control. Six ball transfer units are located on the outer ring of the tail tray. This effectively uses the ring as a bearing and allows low friction rotational motion. In order to provide the required torque and accuracy, we used a Futaba digital servomotor which consumes maximum 12 W. We use a timing belt drive system which has a low power transmission loss.

2.2.3 Ease of Assembly

Ease of assembly is one of the important design criteria. We occasionally need to disassemble the vehicle for routine maintenance and repairs. With the design, the

assembly and disassembly work can all be performed by a single engineer in our laboratory within half an hour.

2.2.4 Effective change of CG

The servomotor has a usable range of 80°. After the pulley ratio, the range reduces to 40°. By placing the IRM at the center, we are able to roll the IRM to ±20°; this translates to an effective change of CG to give a roll of ±5°[1] at equilibrium.

3 Modeling

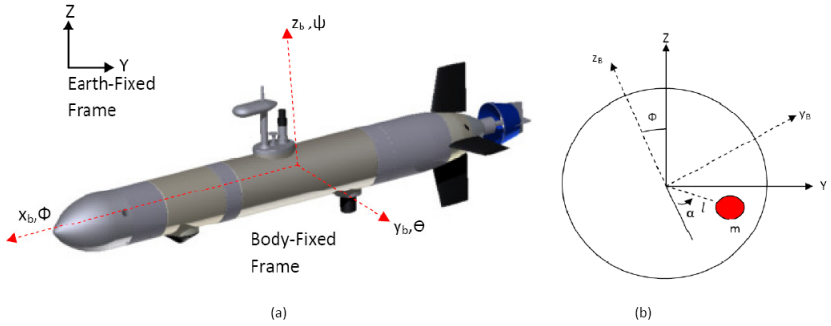

Fig. 2: (a) Coordinate Reference Frame (b) Free Body Diagram.

In this section, we derive the dynamics model for the AUV's roll under consideration of CG shift due to the IRM. A six degree-of-freedom (DOF) dynamics model of an AUV is commonly described by a set of nonlinear equations with respect to two coordinate frames as indicated in Fig. 2(a). Detailed discussion on the modeling can be found in [2, 8]. However, for the purpose of this paper, we restrict our analysis only on rolling motion and treat coupling torque induced by others DOFs to be disturbances.

In Fig. 2(a), we have the body-fixed frame at the center of buoyancy (CB) of the AUV. So the CB is located at $z_b = 0$ and $y_b = 0$ with respect to body-fixed frame. The CG is located below the CB in order to provide righting moment. So the CG location (y_g, z_g) has negative z_g with respect to body-fixed frame.

From Newton's Second Law of Motion (rotation), we can write the net total torque as the product of the moment of inertia I_{xx} and roll angular acceleration $\ddot{\phi}$.

[1] Depending on the vehicle payload configuration, this range might change.

$$\sum \tau = I_{xx}\ddot{\phi}. \tag{1}$$

The sum of the external torque consists of following components:

3.1 Hydrostatic Righting Moment

The hydrostatic righting moment is the combined effect of the vehicle's weight W and buoyancy B. The STARFISH AUV is slightly positively buoyant but as we put the body-fixed frame at the CB, buoyancy does not play a role in the equation. The roll torque due to hydrostatic righting moment is

$$\tau_{Hydro} = -y_g W \cos\phi + z_g W \sin\phi. \tag{2}$$

The IRM is treated as a point mass with effective length l from the center. The effective length l is the distance from the CB to the CG of the tail tray. Let α denote the angular position of the point mass as illustrated in Fig. 2(b). When the point mass is rolling in the AUV, it is effectively changing the CG of the AUV. The new CG position (y'_g, z'_g) is described in following two equations:

$$y'_g = y_g + \frac{m}{M} l \sin\alpha \tag{3}$$

$$z'_g = z_g - \frac{m}{M} l \cos\alpha \tag{4}$$

where m is the mass of tail tray and M is the mass of the whole AUV.

By substituting (3) and (4) into (2), the hydrostatic righting moment becomes

$$\tau_{Hydro} = -(y_g + \frac{m}{M} l \sin\alpha) W \cos\phi + (z_g - \frac{m}{M} l \cos\alpha) W \sin\phi. \tag{5}$$

It is useful to note that the hydrostatic moment stabilizes the roll motion as the moment always acts against any deflection in roll. So the roll dynamics are self-stabilized in this sense.

3.2 Rolling Drag

As a streamlined AUV, the main rolling drag of the STARFISH AUV comes from the four fins that protrude out from the center axis. We model the drag as a quadratic drag:

$$\tau_{Drag} = K_{pp} p |p| \tag{6}$$

where K_{pp} is the rolling quadratic drag coefficient and p is the angular velocity of the roll. Since we restrict our discussion in roll axis only, we have $p = \dot{\phi}$.

3.3 Rolling Added Mass

Added mass is a measure of the mass of the moving water when the vehicle accelerates. For a streamlined AUV, rolling added mass due to the AUV hull is small. So the main rolling added mass is again due to the fins. We model the moment due to the added mass as follows:

$$\tau_{AM} = K_{\dot{p}}\dot{p} \tag{7}$$

where $K_{\dot{p}}$ is the rolling added mass coefficient and $\dot{p}$ is the angular acceleration of roll. Similarly, we have $\dot{p} = \ddot{\phi}$.

3.4 Propeller Induced Torque

When the propeller rotates clockwise to provide the forward thrust, it also creates an anti-clockwise torque acting on the AUV. This is commonly known as the *torque effect*. The magnitude of the torque depends on the power output of the thruster, P and propeller revolution, ω in the following equation:

$$\tau_{prop} = \frac{P}{\omega}. \tag{8}$$

Power produced by the thruster is the product of thrust F, and speed of the AUV V. However during steady state (constant velocity) AUV motion, thrust is equal to the drag force, F_{drag}, and therefore

$$P = FV = F_{drag}V \tag{9}$$

$$F_{drag} = \frac{1}{2}\rho A C_d V^2 \tag{10}$$

where ρ is the sea water density; A is the frontal area; C_d is the drag coefficient. So, by running different constant thrusts experiments, we plot the induced torque against the propeller revolution in Fig. 3. The data best fit a quadratic equation showing $\tau_{prop} \propto \omega^2$.

In our subsequent analysis, we omit the induced torque and treat it as a disturbance to the system. However, we pre-roll the AUV to +5° during weight trimming to compensate for the thruster torque at nominal speed. When the AUV moves at its nominal speed of 1.4 m/s with 1400 rpm, the induced torque will roll back the AUV to zero roll position and thus leave sufficient room for IRM to compensate for the rest of the variations.

By substituting (5), (6), (7) and (8) into (1) and rearranging the terms, we have

$$\begin{aligned}(I_{xx} - K_{\dot{p}})\ddot{\phi} = &-(y_g + \frac{m}{M}l\sin\alpha)W\cos\phi \\ &+(z_g - \frac{m}{M}l\cos\alpha)W\sin\phi\end{aligned}$$

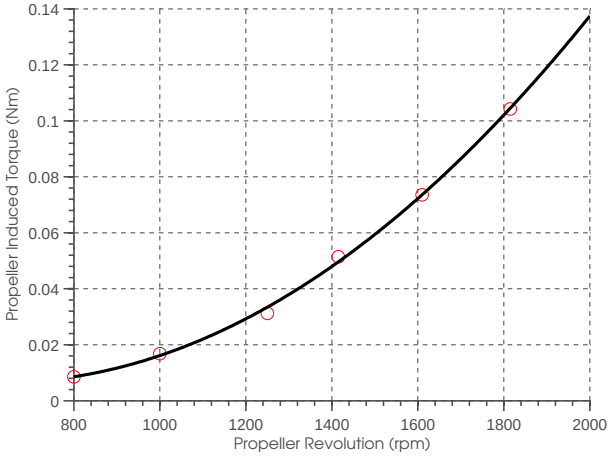

Fig. 3: Propeller induced torque versus propeller revolution

$$+K_{pp}p|p| \\ +\tau_{prop}. \tag{11}$$

We obtain the transfer function of roll ϕ, as a function of α in (12) by first linearizing (11) at the operating point $\phi = 0$. At this point $\cos\phi \simeq 1$ and $\sin\phi \simeq \phi$. α can be assumed to be small. Therefore $\cos\alpha \simeq 1$ and $\sin\alpha \simeq \alpha$. Next, we approximate the quadratic drag $K_{pp}p|p|$ as linear drag $K_p p$. By trimming condition, y_g is close to zero and thus ignored. Lastly, τ_{prop} is treated as disturbance and is not included in the equation.

$$\frac{\phi}{\alpha} = \frac{-\left[\frac{(\frac{m}{M})lW}{I_{xx}-K_{\dot{p}}}\right]}{s^2 - \left[\frac{K_p}{I_{xx}-K_{\dot{p}}}\right]s - \left[\frac{(z_g-(\frac{m}{M})l)W}{l_{xx}-K_{\dot{p}}}\right]}. \tag{12}$$

By assigning the constant parameters k, a, and b to its corresponding coefficient respectively, (12) becomes:

$$\frac{\phi}{\alpha} = \frac{k}{s^2+as+b}. \tag{13}$$

4 System Identification

In this section, we estimate the three unknown parameters a, b and k of the linear second-order roll-axis model presented in (13). We also identify $K_{\dot{p}}$, K_{pp}, and l for nonlinear equation (11). Others parameter such as I_{xx}, y_g, z_g, m, M, W can either be

measured directly or calculated through computer-aided design (CAD) softwares. Numerical values for those parameters are tabulated in Table 1.

Table 1: Model parameters

Calculated Parameters	Values	Identified Parameters	Values
I_{xx}	0.474 kg m^2	a	0.24
y_g	0 mm	b	5.21
z_g	-3.4 mm	k	-0.61
m	2.00 kg	$K_{\dot{p}}$	-0.08 kg m^2
M	61.41 kg	K_{pp}	-1.21 Nms^2
W	602.5 N	l	43.36 mm

Generally, we need to perform open-loop testing by changing α using a step function between $\pm 20^\circ$ and then record the roll response. Ideally, the test should be carried out while the AUV is maintaining constant thrust, depth and heading. This will minimize the coupling torque generated by those degrees of freedom. However, the open loop tests might pose danger to the operation of the AUV as we are testing some unknown behavior of the roll dynamics. A more natural choice would be to carry out the open-loop test while AUV is at rest in a water tank. This turns out to be sufficient to obtain a nominal model for the roll dynamics for the following reasons. First, in our model, we treat the propeller induced torque as a disturbance. So, whether the thruster is running or not, it is not included in the model. Second, the roll dynamics model is derived under a decoupled assumption and therefore it is free from excitation from other axis. Third, the tank test underestimates the drag coefficient as the conning tower and the top fin are not fully submerged in the water. However it is better to underestimate the drag in our case, as higher drag will make the roll dynamics more stable. It will also ensure that the designed controller will also work properly when the vehicle is on the surface before it starts diving.

While the AUV is static in the tank, we command three step inputs of α (-20°, 0° and 20°) and observe how the roll responds to the step change of α. Sufficient time was allowed for the roll response to decay before another step change. The results are shown in Fig. 4. The simulated roll response is overlaid together with the experimental measured roll response. The result shows a good match between the two. The simulated roll is generated from the nonlinear model after the unknowns are identified. The 3 unknown parameters were identified by numerically minimizing the root mean square error ϕ_{rms} defined as:

$$\Phi_{rms} = \sqrt{\frac{\sum_{i=1}^{n}(\phi_i - \hat{\phi}_i)^2}{n}}. \tag{14}$$

where $\hat{\phi}$ is the simulated roll response and n is the number of samples. The Nelder-Mead simplex method was used to search for the optimal parameters set in least square sense.

It is important to note that the α is the command given to the servomotor. There is no instrument to measure the position of the rolling mass. So, some latency is expected between the commanded α and the actual α. We model the latency by a first order system with a time constant τ_{delay}. In order to identify the time constant, we perform a dynamic test by commanding α randomly between $\pm 20^{\circ}$ to obtain the response shown in Fig. 5. Similarly, the time constant is identified by minimizing ϕ_{rms}. The resultant transfer function in (13) becomes:

$$\frac{\phi}{\alpha} = \left(\frac{1}{\tau_{delay}s+1}\right)\left(\frac{k}{s^2+as+b}\right) \tag{15}$$

with $\tau_{delay} = 0.5\ s$.

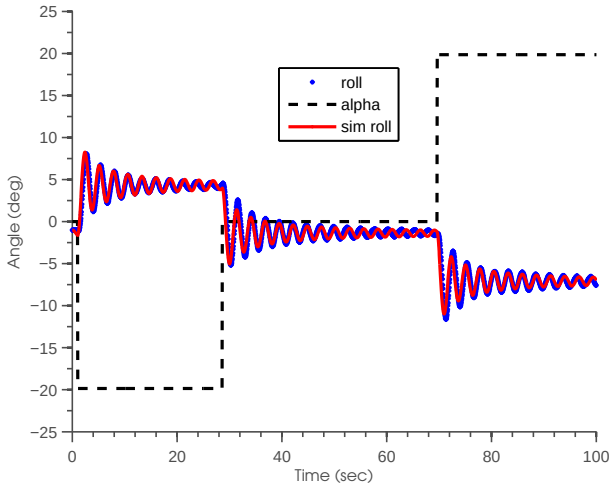

Fig. 4: Simulated and measured roll response under step input. The simulated roll response matched closely with the measured roll response despite small differences in amplitude and phase

5 Controller Design

In this section, we design a Proportional-plus-Integral (PI) controller that stabilizes the AUV's roll motion. The PI controller is used to reduce the roll oscillation by increasing the damping of the system and at the same time maintain zero steady state error. The controller was synthesized base on root locus design (Fig. 6).

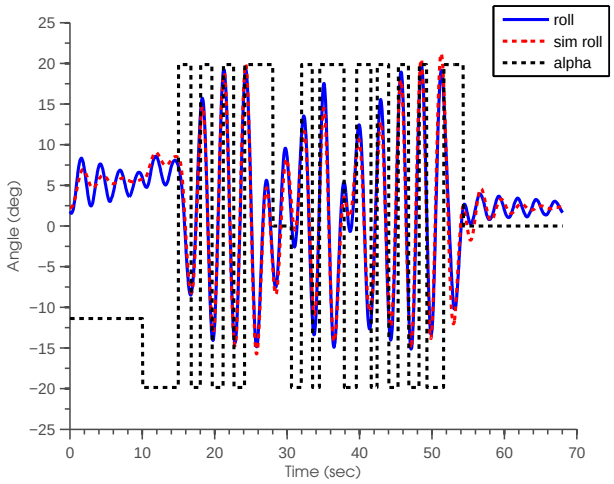

Fig. 5: Simulated and measured roll response under random input.

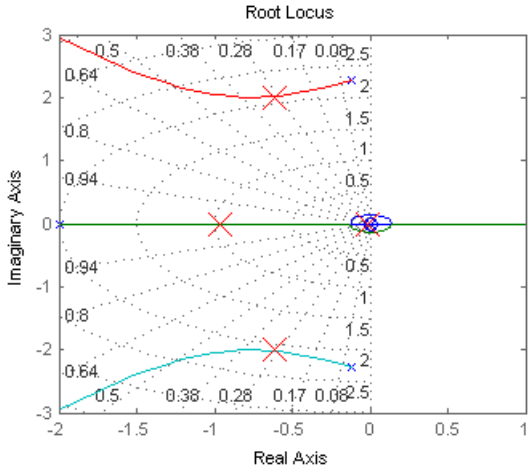

Fig. 6: Root locus plot for compensated system.

The open loop transfer function has a pair of complex-conjugate *poles* close to the imaginary axis in the s-plane. This indicates the system is lightly damped with a damping ratio of 0.07. Fig. 6 also shows that the system is only stable for a small region of the root locus; it is stable for closed-loop gain range between $(0 < Kp < 8.50)$. The portion that is stable appears to be lightly damped as well. By increasing the gain, we bring the pair of complex-conjugate *poles* to a region of higher damping. However, the third *pole* moves closer to the right-half plane as the gain increases. As the *poles* are close to each other, we cannot analyze the system

purely based on a second-order approximation. Instead, we simulate the nonlinear model and fine tune the controller gain using the simulation results. An ideal integral was added with a *zero* at 0.01. The fourth closed-loop *pole* is found at -0.0144, close enough to the *zero* to cause *pole-zero* cancellation. All *poles* and *zero* of the open and closed-loop plant are tabulated in Table 2. Integrator windup is avoided by preventing the integral term from accumulating above or below 20°.

Table 2: Open and Closed Loop Plants

	Open loop	Closed loop
Plant	$\frac{K}{(s+2)(s^2+0.24s+5.21)}$	$\frac{K(s-0.01)}{s(s+2)(s^2+0.24s+5.21)}$
K	-1.22	-6.10
Kp	-	5
Poles	$-0.12+2.2794i$	$-0.617+2.0077i$
	$-0.12+2.2794i$	$-0.617+2.0077i$
	-2	-0.9609
		-0.0144
Zeros	-	0.01
System Type	0	1

6 Result and Discussion

The performance of the internal rolling mass in controlling the roll was first studied in a tank test and later at an open-field trial. For the tank test, we gave an impulse to the AUV by pushing AUV to roll to 25° and observed how the roll decays for open-loop and closed-loop control respectively. The results are shown in Fig. 7. The closed-loop response settle down within 4 seconds whereas the open-loop system takes more than 10 seconds to settle down. Fig. 7 also shows how the α changes with time in order to damp down the roll. For the open-loop test, α was kept at a constant 0°.

Fig. 8 shows the AUV's roll response during a constant 2 m diving mission at the speed of 1.4 m/s when traveling on a straight path. When the IRM mechanism was turned off (open loop), the AUV's roll response was oscillatory with standard deviation of 1.02°. On the contrary, when the IRM mechanism was turned on (closed loop), the oscillatory roll motion was damped. The moving mass rolls to negative alpha region to neutralize the induced propeller torque. The standard deviation of roll reduced to 0.393°. Table 3 summarizes the test results into two statistics: mean and standard deviation. Looking at the mean value, the IRM mechanism also made oscillation centered at zero angle. In short, the result shows that the IRM mechanism suppressed the unwanted roll oscillation to a smaller amplitude with center around zero.

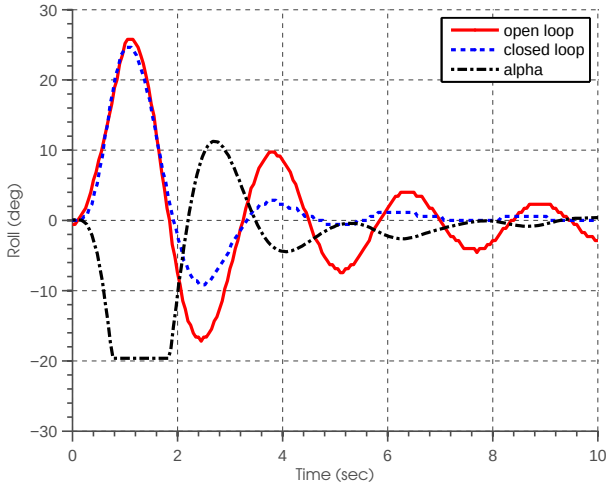

Fig. 7: Tank Test Result. The result shows that despite actuator saturation, the IRM mechanism manages to damp down the oscillation faster.

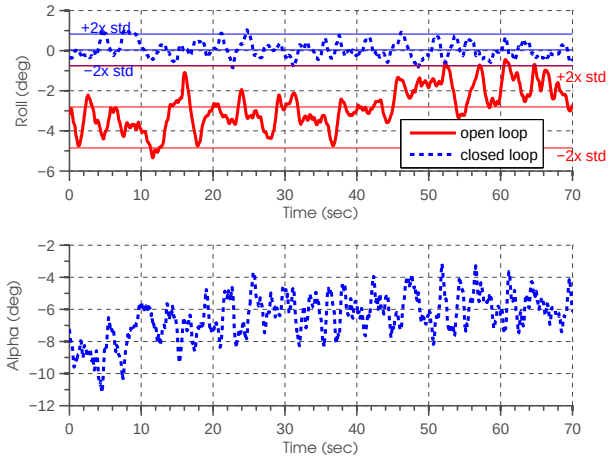

Fig. 8: Open Field Test Result.

7 Conclusions

We demonstrated the use of an internal rolling mass (IRM) mechanism for active roll stabilization in a tail-thrusted and fin-controlled AUV. The mechanism was designed and implemented in the STARFISH AUV. A nonlinear model was first developed to describe the dynamics of the AUV's roll. The model was later linearized to obtain a transfer function for controller synthesis. The model's parameters were identified

Table 3: Open and Closed Loop Performance

	Open loop	Closed loop
Mean	-2.808 °	0.039 °
Standard Deviation	1.023 °	0.393 °

through open-loop testing in the water tank. A PI controller was then designed to increase the overall system damping and remove the steady state error. The capability of IRM to stabilize the roll motion was demonstrated in a tank test as well as through open-field tests.

References

[1] Alvarez A, Caffaz A, Caiti A, Casalino G, Gualdesi L, Turetta A, Viviani R (2009) Folaga: a low-cost autonomous underwater vehicle combining glider and auv capabilities. Ocean Engineering 36(1):24–38

[2] Fossen T (1994) Guidance and control of ocean vehicles. New York

[3] Kirkwood W, Anderson WR, Kitts C (2009) Fault tolerant actuation for dorado class, auvs. Instrumentation viewpoint (8):40–41

[4] Koay T, Tan Y, Eng Y, Gao R, Chitre M, Chew J, Chandhavarkar N, Khan R, Taher T, Koh J (2011) Starfish–a small team of autonomous robotic fish. IJMS 40:157–167

[5] Leonard N, Graver J (2001) Model-based feedback control of autonomous underwater gliders. Oceanic Engineering, IEEE Journal of 26(4):633–645

[6] McEwen R, Streitlien K (2001) Modeling and control of a variable-length auv. Proc 12th UUST

[7] Petrich J, Stilwell D (2010) Robust control for an autonomous underwater vehicle that suppresses pitch and yaw coupling. Ocean Engineering

[8] Prestero T (2001) Verification of a six-degree of freedom simulation model for the remus autonomous underwater vehicle. Master's thesis, Massachusetts Institute of Technology and Woods Hole Oceanographic Institution

[9] Singh H, Whitcomb L, Yoerger D, Pizarro O (2000) Microbathymetric mapping from underwater vehicles in the deep ocean. Computer Vision and Image Understanding 79(1):143–161

[10] Woock P (2011) Deep-sea seafloor shape reconstruction from side-scan sonar data for auv navigation. In: OCEANS, 2011 IEEE-Spain, IEEE, pp 1–7

[11] Woolsey C, Leonard N (2002) Moving mass control for underwater vehicles. In: American Control Conference, 2002. Proceedings of the 2002, IEEE, vol 4, pp 2824–2829